COBEM-2017-0179
EFFECT OF THE FLOW MACRO-SCALE ON THE EFFECTIVE STRESSES IN GAS-SOLID RISER FLOWS

Joseph MOUALLEM
Seyed Reza Amini NIAKI
Norman CHAVEZ
Gabriel J. S. NETZALAFF
Christian C. MILIOLI
Fernando E. MILIOLI
Department of Mechanical Engineering, School of Engineering of Sao Carlos, University of Sao Paulo, 13566-590 Sao Carlos-SP, Brazil
josephmouallem@usp.br, r.amini@usp.br, normanchavez@usp.br, gabriel.netzalaff@usp.br, ccosta@sc.usp.br, milioli@sc.usp.br

Abstract. The two-fluid modeling approach usually applied in large scale simulation of gas-particle riser flows requires closure models to deal with sub-grid filtered parameters such as effective stresses and interphase interactions. The very heterogeneous riser flows are characterized by a continuous intense formation and dissipation of particulate coherent structures. In spite of this complex topology, two-fluid modeling, where fluid and particulate are treated as interpenetrating continua, does provide qualitatively correct solutions. The current approaches, however, still cannot deliver quantitative accuracy, mostly owing to the lack of more accurate sub-grid filtered models. The effective stresses in both the phases are among the sub-grid filtered parameters for which model enhancement is required. Models for effective stresses have been recently derived from filtering over results of highly resolved simulations with two-fluid modeling. Those models account for sub-grid flow heterogeneities, but disregard any macro-scale topology effect. This work shows that effective stresses modeling also requires correlation to macro-scale effects, the domain average solid volume fraction and the domain average gas flow Reynolds number being relevant macro-scale parameters to be accounted for.

Keywords: multiphase flow, gas-solid flows, two-fluid model, CFD, MFIX

1. INTRODUCTION

Gas-particle riser flows are characterized by very heterogeneous patterns dominated by continuous formation and dissipation of particulate coherent structures. Two-fluid modeling, where gas and particulate are treated as interpenetrating continua, is widely used in large scale simulations of such flows (e.g. Gidaspow, 1994). While this approach can provide qualitative good macro-scale descriptions, quantitative accuracy is still out of reach. One reason for that is the lack of accurate models to properly describe sub-grid filtered parameters that are required for closure in large scale simulations. Among the closures that require enhancement are those for effective stresses on both phases and interphase interactions. This article is intended to be a contribution in that context by discussing possible sub-grid modeling enhancement for effective stresses.

The two-fluid model approach in its formulation suitable to large scale simulations, also known as filtered two-fluid model, does require closures for the Reynolds like or effective stresses in both the phases. Such closures, which are usually cast in terms of effective pressures and dynamic viscosities, have been derived empirically as well as theoretically, from results of highly resolved simulations with the so called microscopic two-fluid modeling approach. The empiricism has provided various correlations for the effective pressure and viscosity of solid phases (see, for instance, Gidaspow and Ettehadieh, 1983; Bouillard et al., 1989; Tsuo and Gidaspow, 1990; Sinclair and Jackson, 1989; Campbell and Wang, 1991; Massoudi et al., 1992; Gidaspow, 1994; Enwald et al., 1996; Sinclair, 1997). Those effective parameters are frequently formulated accounting for effects of momentum transfers due to particle velocity fluctuations (kinetic effect), collisional and long enduring contacts among particles (contact effects), and damping on particulate motion by the interstitial gas (gas pressure effect). As for the gas phase, effective pressures and viscosities have been taken mostly as constants, and also by considering some monophase turbulence model (see, for instance, Hrenya and Sinclair, 1997).

Effective pressures and viscosities have also been derived from filtering over results of highly resolved simulations with microscopic two-fluid modeling. Such microscopic formulation requires closures for viscous stresses which come from the conventional Newtonian fluid assumption for both the phases. Regarding the gas phase, pressure comes out from the usual combination of continuity and momentum equations, dynamic viscosity is taken constant, and bulk viscosity is

disregarded as lower order. As for the solid phase, pressure, dynamic viscosity and bulk viscosity are all brought from the kinetic theory of granular flows (Jenkins and Savage, 1983; Lun et al., 1984; Garzó and Dufty, 1999; Gidaspow, 1994). This is an analogy with the kinetic theory of dense gases, which allows for the determination of fluid properties such as viscosity and pressure as a function of the thermodynamic temperature. Following the analogy, the kinetic theory of granular flows allows for the determination of a granular viscosity and a granular pressure (usually called solid phase viscosity and pressure) as a function of a granular temperature. A granular energy conservation equation provides for a granular temperature field in an analogous way as the energy conservation equation provides for a thermodynamic temperature field. A number of works have been developed which provided effective stresses analyses and correlation departing from results of highly resolved simulations with microscopic two fluid modeling (Agrawal et al., 2001; Andrews IV et al., 2005; Igci et al., 2008; Milioli and Milioli, 2011; Igci and Sundaresan, 2011a,b; Parmentier et al., 2012; Ozel et al., 2013; Milioli et al., 2013; Agrawal et al., 2013; Schneiderbauer and Pirker, 2014; Sarkar et al., 2016). In general, the highly resolved simulations provide meso-scale solutions over which filtering is performed to provide sub-grid filtered data for parameters such as the effective pressures and viscosities of both phases. At the current state of affairs, those effective parameters are correlated to inside filter averaged parameters only, disregarding any effects of the outside flow topology.

All the different correlations and proposals to deal with effective pressures and viscosities have partially succeeded in different ad-hoc situations. However, generalization and accuracy are still to be met. In the present work, the procedure for generating the concerning sub-grid parameters based on highly resolved simulations with microscopic two-fluid modeling is taken one step ahead, by investigating the relevance of macro-scale effects which were previously disregarded. While the sub-grid heterogeneities of the flow are accounted for in the current sub-grid models, any macro-scale effects associated to the flow topology are disregarded. This work shows that the modeling of effective pressures and viscosities should also include correlation to the macro-scale flow topology, in addition to usual correlation to sub-grid filtered effects. The domain average solid volume fraction and the domain average gas flow Reynolds number have been showed to be relevant macro-scale parameters to be accounted for.

2. METHOD

Large scale simulations of gas-particle riser flows can be performed by applying filtered two-fluid modeling. This approach requires sub-grid closures that can be derived from results of highly resolved simulations with microscopic two-fluid modeling. There is a considerable literature describing two-fluid modeling applied to gas-particle fluidized flows (Anderson and Jackson, 1967; Gidaspow, 1994; Enwald et al., 1996). Both the filtered and microscopic formulations of the two-fluid model are described next, in order to show where the sub-grid closures are needed, and the referred means by which they are derived.

2.1 Microscopic Two-Fluid model

The microscopic formulation of the two-fluid model as applied to gas-particle fluidized flows is partially presented in "Tab. 1", emphasizing the formulation of main concern in the present work. The micro-scale closures for the solid phase stresses are established by applying the kinetic theory of granular flows (KTGF) (Jenkins and Savage, 1983; Lun et al., 1984; Gidaspow, 1994; Garzo et al., 1999), where the continuous solid phase micro-scale properties are derived as a function of a granular temperature determined from a pseudo thermal energy balance. These closures are the same as the ones assumed by Agrawal et al., 2001. In addition to the conservative equations of continuity and momentum, the microscopic model also requires a conservation equation of granular energy to be resolved as well (Gidaspow, 1994; Agrawal, 2001). "Equations (2.1), (2.2), (2.3), and (2.4)" represent the continuity and momentum conservation equations for the gas and solid phases. "Equation (2.5)" represents the volumetric continuity. "Equation (2.6)" represents the conservation of granular energy. Closures for the stresses are presented next in the table. Other closures (for the granular energy conservation, and interface forces) can be found in (Mouallem et al., 2017).

Table 1: Two-fluid model

Continuity and momentum conservation equations :

$$\frac{\partial}{\partial t}(\rho_g \phi_g) + \nabla \cdot (\rho_g \phi_g \mathbf{v}_g) = 0 \tag{2.1}$$

$$\frac{\partial}{\partial t}(\rho_s \phi_s) + \nabla \cdot (\rho_s \phi_s \mathbf{v}_s) = 0 \tag{22}$$

$$\frac{\partial}{\partial t}(\rho_g \phi_g \mathbf{v}_g) + \nabla \cdot (\rho_g \phi_g \mathbf{v}_g \mathbf{v}_g) = -\phi_g \nabla \cdot \boldsymbol{\sigma}_g - \mathbf{M}_I + \rho_g \phi_g \mathbf{g} \tag{23}$$

$$\frac{\partial}{\partial t}(\rho_s \phi_s \mathbf{v}_s) + \nabla \cdot (\rho_s \phi_s \mathbf{v}_s \mathbf{v}_s) = -\nabla \cdot \boldsymbol{\sigma}_s - \phi_s \nabla \cdot \boldsymbol{\sigma}_g + \mathbf{M}_I + \rho_s \phi_s \mathbf{g} \tag{24}$$

Volumetric continuity :

$$\phi_g + \phi_s = 1 \tag{25}$$

Granular energy conservation equation :

$$\frac{3}{2}\left[\frac{\partial}{\partial t}(\rho_s \phi_s \Theta) + \nabla \cdot (\rho_s \phi_s \mathbf{v}_s \Theta)\right] = -\boldsymbol{\sigma}_s : \nabla \mathbf{v}_s + \nabla \cdot (\kappa_s \nabla \Theta) + \Gamma_{slip} - J_{coll} - J_{vis} \tag{26}$$

Closure for stresses :

$$\boldsymbol{\sigma}_l = \left[P_l - \left(\lambda_l + \frac{2}{3}\mu_l\right)(\nabla \cdot \mathbf{v}_l)\right]\mathbf{I} - 2\mu_s \boldsymbol{s}_l \qquad l = g, s \tag{27}$$

$$\boldsymbol{s}_l = \frac{1}{2}\left[\nabla \mathbf{v}_l + (\nabla \mathbf{v}_l]^T\right) - \frac{1}{3}(\nabla \cdot \mathbf{v}_l)\mathbf{I} \qquad l = g, s \tag{28}$$

$$\mu_g = constant \qquad \lambda_g = 0 \tag{29}$$

$$\mu_s = \frac{(2+\alpha)}{3}\left\{\frac{\xi^*}{g_0 \eta (2-\eta)}\left(1 + \frac{8}{5}\phi_s \eta g_0\right)\left(1 + \frac{8}{5}\eta(3\eta - 2)\phi_s g_0\right) + \frac{6}{5}\eta \mu_b\right\} \tag{2.10}$$

$$\lambda_s = \eta \mu_b - \frac{2}{3}\mu_s \qquad \alpha = 1.6 \tag{2.11}$$

$$\mu_b = \frac{256\xi\phi_s^2 g_0}{5\pi} \qquad \xi^* = \frac{\xi}{1 + \frac{2\beta\xi}{(\rho_s\phi_s)^2 g_0 \Theta}} \qquad \xi = \frac{5\rho_s d_p(\pi\Theta)^{\frac{1}{2}}}{96} \tag{2.12}$$

$$P_s = \rho_s \phi_s (1 + 4\eta\phi_s g_0)\Theta \tag{2.13}$$

$$g_0 = \frac{1}{1 - \left(\frac{\phi_s}{\phi_{s,max}}\right)^{\frac{1}{3}}} \qquad \phi_{s,max} = 0.65 \qquad \eta = \frac{1+e}{2} \tag{2.14}$$

Other required closures can be found in (Mouallem et al., 2017)

2.2 Filtered Two-Fluid model

The two-fluid microscopic equations can be transformed into coarse-grained (or filtered) equations through filtering, using spatial averaging (weighting function) over a certain length scale (filter size). This procedure provides the filtered two-fluid model presented in "Tab. 2".

In these filtered equations, filtered microscopic effects appear which require constitutive formulations to close the set of equations. Regarding the effective stresses of main interest in the present work, the terms that require closure are the particle phase effective pressure and viscosity, represented by "Eq (222) and (223)" respectively. Just as done for the microscopic model given in "Tab. 1", the filtered model in "Tab. 2" is only presented partially, emphasizing the formulation of main concern in the present work. Further closures for the filtered model can be found in (Mouallem et al., 2017)

Table 2: Filtered two-fluid model

Filtered continuity and momentum conservation equations:

$$\frac{\partial}{\partial t}\left(\rho_g \overline{\phi}_g\right) + \nabla \cdot \left(\rho_g \overline{\phi}_g \widetilde{\mathbf{v}}_g\right) = 0 \tag{2.15}$$

$$\frac{\partial}{\partial t}\left(\rho_s \overline{\phi}_s\right) + \nabla \cdot \left(\rho_s \overline{\phi}_s \widetilde{\mathbf{v}}_s\right) = 0 \tag{2.16}$$

$$\frac{\partial}{\partial t}\left(\rho_g \overline{\phi}_g \widetilde{\mathbf{v}}_g\right) + \nabla \cdot \left(\rho_g \overline{\phi}_g \widetilde{\mathbf{v}}_g \widetilde{\mathbf{v}}_g\right) = -\overline{\phi}_g \nabla \widetilde{\boldsymbol{\sigma}}_g - \nabla \cdot \boldsymbol{\tau}'_g - \left(\mathbf{B}'_{gs} + \overline{\mathbf{M}}_I\right) + \rho_g \overline{\phi}_g \mathbf{g} \tag{2.17}$$

$$\frac{\partial}{\partial t}\left(\rho_s \overline{\phi}_s \widetilde{\mathbf{v}}_s\right) + \nabla \cdot \left(\rho_s \overline{\phi}_s \widetilde{\mathbf{v}}_s \widetilde{\mathbf{v}}_s\right) = -\nabla \cdot \overline{\boldsymbol{\sigma}}_s - \nabla \cdot \boldsymbol{\tau}'_s - \overline{\phi}_s \nabla \cdot \widetilde{\boldsymbol{\sigma}}_g + \left(\mathbf{B}'_{gs} + \overline{\mathbf{M}}_I\right) + \rho_s \overline{\phi}_s \mathbf{g} \tag{2.18}$$

Filtered volumetric continuity:

$$\overline{\phi}_g + \overline{\phi}_s = 1 \tag{2.19}$$

Closure for effective stresses :

$$\boldsymbol{\tau}'_\ell = \rho_\ell \overline{\phi}_\ell (\mathbf{v}_\ell \mathbf{v}_\ell) + \rho_\ell \overline{\phi}_\ell \widetilde{\mathbf{v}}_\ell \widetilde{\mathbf{v}}_\ell = P_{eff,\ell}\mathbf{I} - 2\mu_{eff,\ell}\widetilde{\mathbf{s}}_\ell \qquad \text{for} \qquad \ell = g,s \tag{2.20}$$

$$\widetilde{\mathbf{s}}_\ell = \frac{1}{2}\left(\nabla \widetilde{\mathbf{v}}_\ell + (\nabla \widetilde{\mathbf{v}}_\ell)^T\right) - \frac{1}{3}\left(\nabla \cdot \widetilde{\mathbf{v}}_\ell\right)\mathbf{I} \qquad \text{for} \qquad \ell = g,s \tag{2.21}$$

$$P_{eff,\ell} = \frac{1}{3}tr(\boldsymbol{\tau}'_\ell) \qquad \text{for} \quad \ell = g,s \tag{2.22}$$

$$\mu_{eff,\ell} = \frac{|\boldsymbol{\tau}'_{shear,\ell}|}{2|\widetilde{\mathbf{s}}_{shear,\ell}|} \tag{2.23}$$

Other required closures can be found in (Mouallem et al.,2017

2.3 Numerical Simulations

Numerical simulations were performed using the open source Fortran code MFIX (Syamlal et al.,1993; Syamlal et al.,1998). Two-dimensional periodic boundaries were applied for a 16 cm x 16 cm domain size. According to literature (Agrawal et al., 2001), a grid size between 1 and 2 mm provides grid size independent results. Following this, a numerical mesh of 128x128 was used, resulting in a grid size of 1.25 mm.

The domain average gas Reynolds number, fixed in each simulation, is given by:

$$Re_p = \frac{d_p \rho_g \langle \phi_g \rangle \langle V_{g,y} \rangle}{\mu_g} \tag{2.24}$$

Where $\langle v_{g,y} \rangle$ represents the domain averaged gas phase velocity in the axial (vertical) direction. The domain average solid volume fraction $\langle \phi_s \rangle$ was also set constant in the various simulations, at the values of 0.05, 0.15 and 0.25. For each domain averaged solid volume fraction, the domain average gas Reynolds number was calculated for the suspension case. A suspension simulation consists of applying a pressure gradient in the vertical direction to exactly balance the weight of the gas and solid mixture existing in the domain:

$$\frac{\Delta P_y}{L} = \rho_s \langle \phi_s \rangle g + \rho_g \langle \phi_g \rangle g \tag{2.25}$$

After calculating the suspension case domain average gas Reynolds number $\langle Re_g \rangle_{susp}$, the actual $\langle Re_g \rangle$ is set fixed in each simulation by composing a ratio $\langle Re_g \rangle / \langle Re_g \rangle_{susp}$ = 1.00, 4.08, 8.15, 12.23, 16.30, 20.34, and 24.45 for each $\langle \phi_s \rangle$ considered.

In all the simulations, the particle diameter $d_p = 7.5\text{x}10^{-5}m$, the particle density $\rho_s = 1.3 kg/m^3$, the gas density $\rho_g = 1.3 kg/m^3$, the gas viscosity $\mu_g = 1.8\text{x}10^{-5} kg/m.s$, the coefficient of restitution $e_p = 0.9$. From those properties, the terminal settling velocity of a particle $v_t = 0.2184 m/s$, and the particle Froude number $Fr = v_t^2/(gd_p) = 64.85$.

2.4 Filtering procedure

"Figure 1" presents the domain averaged gas phase velocity in the axial (vertical) direction, $\langle V_{g,y} \rangle$, as a function of time, up to 15s of simulation. A transient regime can be noticed from $t = 0s$ until about $t = 1s$. Beyond that, the so called statistical steady state regime begins. In this regime, the average in time and space are statistically equivalent, and all space averages vary in time around a well established average. The filtering process is done only while the simulation is in the statistical steady state regime.

For all the cases considered, the statistical steady state was already established at $t = 1$, and filtering was performed from this time up to $t = 10s$ of real time simulation. This time interval was found enough to provide robust statistics for all the cases.

The filtering process is illustrated in "Fig. 2". A square window of $1cm$ x $1cm$ was used in the present work. "Figure 2"
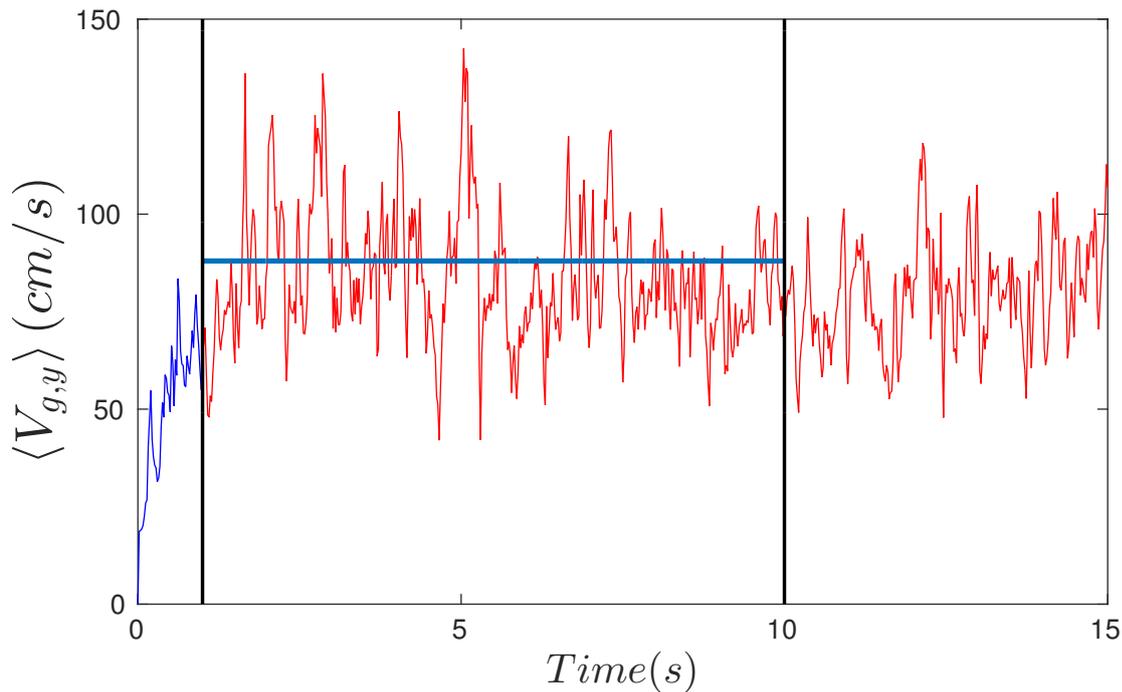
Figure 1: Domain average gas phase axial (vertical) velocity for the suspension case simulation under $\langle \phi_g \rangle = 0.05$.

represents a snapshot of the solid volume fraction in a periodic domain, with one particular filter size comprising a number of grid cells, for a simulation under suspension-like conditions. All the regions in this figure are statistically equivalent. The filter window is made to sweep all over the domain while averages of variables are determined among the internal numerical cells. A large amount of data can be gathered from every instantaneous snapshot.

The filtered results were gathered as a function of the filtered slip velocity and the filtered average particle volume fraction following (Milioli et al., 2013). In each filtered region, properties like the phase velocities were calculated and placed in appropriate bins, defined by ranges of filtered solid volume fraction and filtered slip velocity. While storing the filtered data inside the bins, they are simultaneously ensemble averaged.
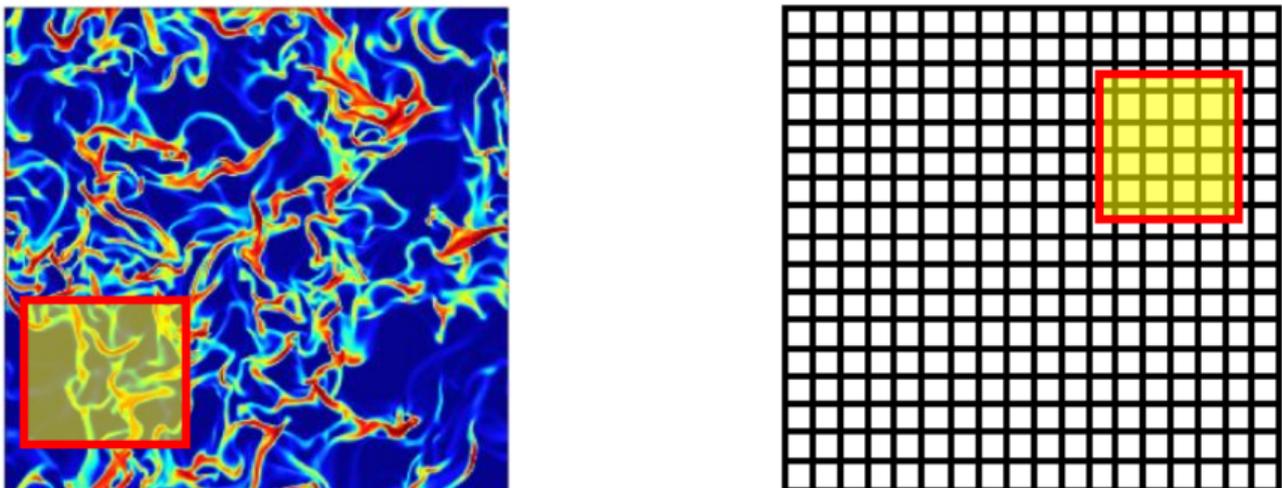

Figure 2: Illustration of a snapshot of solid volume fraction field and numerical grid from a typical 2D periodic simulation of a dilute gas-solid flow, showing a filtering window that sweeps through providing for average filtered data.

3. Results and discussion

Simulations that were performed provide results for various ranges of indepedent variables (i.e. filtered solid volume fraction and filtered velocity), while various filter sizes can be applied on filtering. However, the effects of those trends have already been extensively analyzed in previous works (Igci et al., 2011; Milioli et al., 2013; Sarkar et al., 2016). Owing to that, and considering that the main concern in this work is turned to macro-scale effects, results are here presented only for unique dimensionless filtered slip velocity $\tilde{v}_{\text{slip,y}}/v_{\text{t}} = 0.84$, and the dimensionless filter size $\Delta_{\text{f}}/(v_{\text{t}}^2/g) = 2.056$. The effective pressures and viscosities of concern are made dimensionless by the amount $\rho_s v_t^2$ and $\rho_s v_t^3/g$, respectively.

"Figures 3a, 3b, and 3c" show the variation of the effective solid and gas pressures, $P_{eff,s}$ and $P_{eff,g}$, for domain average solid volume fractions $\langle \phi_s \rangle = 0.05, 0.15$ and 0.25, respectively, as a function of the filtered solid volume fraction $\overline{\phi}_s$, for Reynolds number ratios varying from 1.00 to 24.45. As seen, the domain average gas Reynolds number has a significant effect over the effective pressures for both phases. A noticeable variation can be seen for $\langle \phi_s \rangle = 0.15$ and 0.25, especially for $\overline{\phi}_s < 0.2$. Variations of up to two orders of magnitude can be observed.

"Figure 3d" presents the effective pressure P_{eff} of both phases for $\langle \phi_s \rangle = 0.05, 0.15$ and 0.25, and Reynolds number ratios $1, 12.23$ and 24.45. For both phases, small differences can be seen between the profiles for $\langle \phi_s \rangle = 0.15$ and 0.25 at low Reynolds number ratios. The difference increases for the higher Reynolds ratio 24.45. Very remarkable difference among the profiles can be observed for the high Reynolds ratio 24.45, when the results for $\langle \phi_s \rangle = 0.15$ and 0.25 (symbols) are compared to those for $\langle \phi_s \rangle = 0.05$ (lines) . One possible explanation for this behavior can be related to the increased degree of homogeneity of a dilute flow at high Reynolds numbers.

"Figures 4a, 4b, and 4c" show the variation of the effective solid and gas viscosities , $\mu_{eff,s}$ and $\mu_{eff,g}$ for the same conditions in 3, that is for domain average solid volume fractions $\langle \phi_s \rangle = 0.05, 0.15$ and 0.25, respectively, as a function of the filtered solid volume fraction $\overline{\phi}_s$, for Reynolds number ratios varying from 1.00 to 24.45. The effective viscosities of both phases are notably affected by the domain average gas Reynolds number for all domain average solid volume fractions, especially for low $\overline{\phi}_s$. Variations up to one order of magnitude can be easily noticed in some cases.
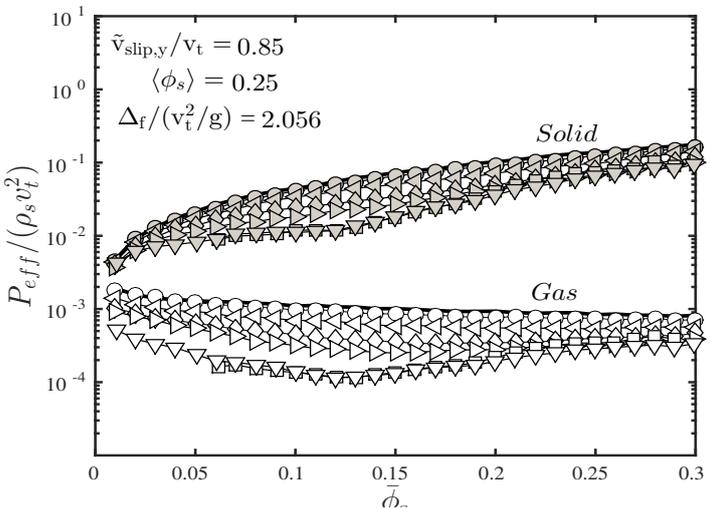
"Figure 4d" presents the effective viscosity μ_{eff} of both phases for the same conditions in "Fig. 3d". In contrast with the behavior seen for P_{eff} in "Fig. 3d", when passing from $\langle \phi_s \rangle = 0.15, 0.25$ to $\langle \phi_s \rangle = 0.05$, under the high Reynolds number ratio of 24.45, the differences among the profiles are relatively small for both phases.
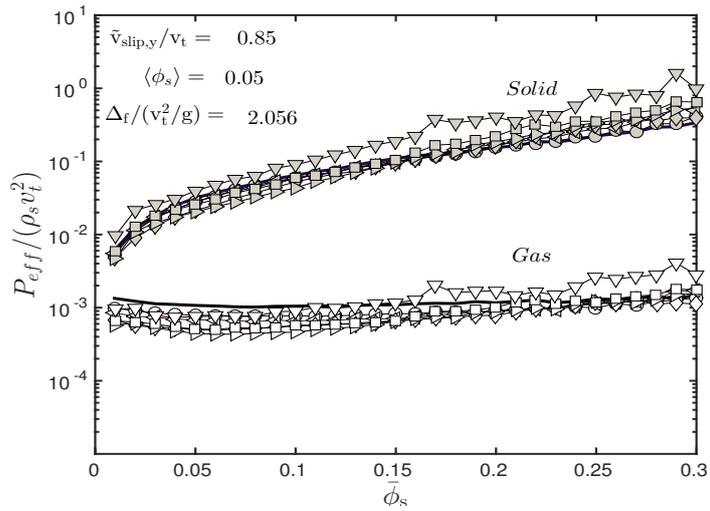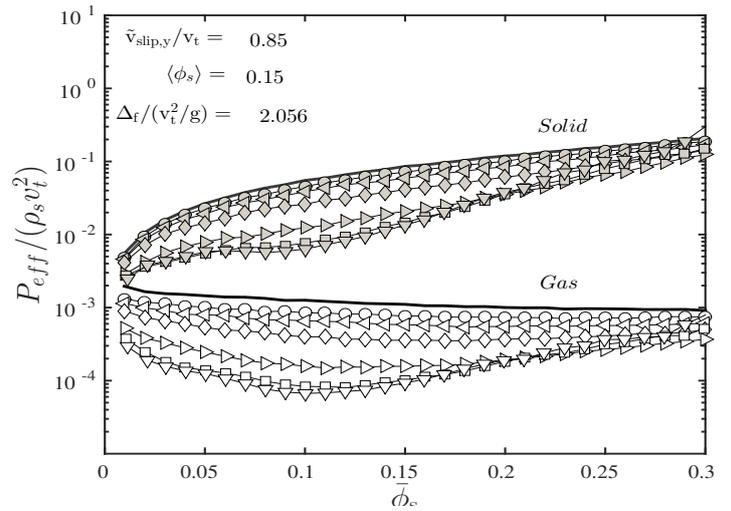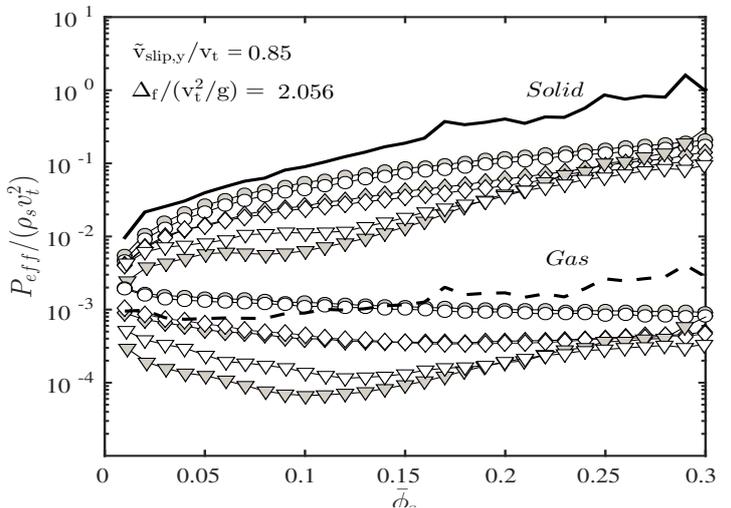
Figure 3: Effective solid and gas pressures, $P_{eff,s}$ and $P_{eff,g}$, as a function of the filtered solid volume fraction, $\overline{\phi}_s$, for various gas Reynolds ratios $\langle Re_g \rangle / \langle Re_g \rangle_{susp} = 1(-), 4.08(\circ), 8.15(\triangleleft), 12.23(\diamond), 16.30(\triangleright), 20.34(\square)$, and $24.45(\triangledown)$, for the domain average solid volume fraction $\langle \phi_s \rangle = 0.05$ (a), 0.15 (b) and 0.25 (c). For figure 3d, the domain average solid volume fractions $\langle \phi_s \rangle = 0.05$ (lines), 0.15 (gray symbols) and 0.25 (white symbols), for various gas Reynolds ratios $\langle Re_g \rangle / \langle Re_g \rangle_{susp} = 1(\circ), 12.23(\diamond)$, and $24.45(\triangledown)$. The lines stand for $\langle Re_g \rangle / \langle Re_g \rangle_{susp} = 24.45$ (full lines for the solid phase; dashed lines for the gas phase)
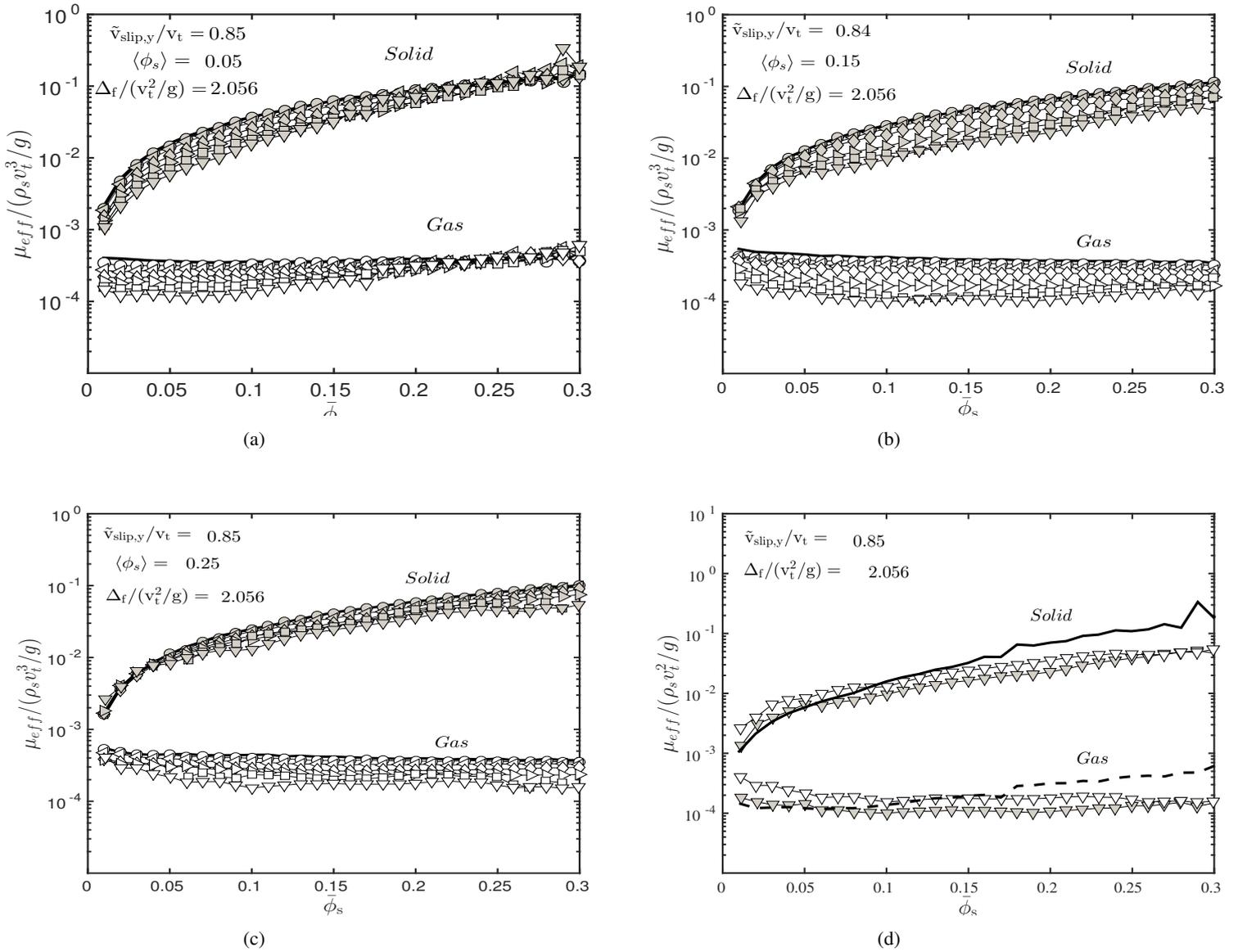
Figure 4: Effective solid and gas dynamic viscosities, $\mu_{eff,s}$ and $\mu_{eff,g}$, as a function of the filtered solid volume fraction, $\overline{\phi}_s$, for various gas Reynolds ratios $^{\langle Re_g \rangle}/_{\langle Re_g \rangle_{susp}} = 1(-), 4.08(\circ), 8.15(\triangleleft), 12.23(\diamond), 16.30(\triangleright), 20.34(\square)$, and $24.45(\triangledown)$, for the domain average solid volume fraction $\langle \phi_s \rangle = 0.05$ (a) , 0.15 (b) and 0.25 (c). For figure 4d: the domain average solid volume fractions $\langle \phi_s \rangle = 0.05$ (lines), 0.15 (gray symbols) and 0.25 (white symbols), gas Reynolds ratios $^{\langle Re_g \rangle}/_{\langle Re_g \rangle_{susp}} = 24.45(\triangledown)$ (full lines for the solid phase; dashed lines for the gas phase).

4. Conclusions

Sub-grid closure models are required for macro-scale simulations of gas-solid riser flows, which can be derived from results of highly resolved simulations with microscopic two-fluid modeling. Among such closures are those for effective pressures and viscosities of both gas and solid phases.

In order to contribute to the development of better closures for effective pressures and viscosities, the effect of a new system variable over the filtered parameters is investigated. In this work, the effect of the macro-scale gas Reynolds number over the effective pressure and viscosity of the two phases has been explored.

2D highly resolved simulations with microscopic two-fluid modeling were performed using the Fortran open source code MFIX. Periodic boundaries in all directions were applied over a domain size of 16x16 cm. Filtering was considered in the statistical steady state flow regime, over a large enough time interval. Gas Reynolds number were varied from 1.00 to 24.45 times the gas Reynolds number required for the suspension case. The effective pressure and viscosity results were also inspected for specific domain average solid volume fractions.

A significant effect of the macro-scale gas Reynolds number was detected over the parameters in question, especially

for very high Reynolds numbers. In addition, in the dilute case, some remarkable variation of behavior was noticed possibly due to the change of flow topology at high Reynolds numbers.

5. ACKNOWLEDGEMENTS

6. REFERENCES

Agrawal, K., Loezos, P.N., Syamlal, M. and Sundaresan, S., 2001, *"The role of meso-scale structures in rapid gas-solid flows"* , J. Fluid Mech., Vol. 445, pp. 151-185.

Agrawal, K., Holloway, W., Milioli, C.C., Milioli, F.E. and Sundaresan, S., 2013, *"Filtered models for scalar transport in gas-particle flows"*, Chem. Eng. Science, Vol,. 95, pp. 291-300.

Anderson, T.B. and Jackson, R., 1967, *"Fluid Mechanical Description of Fluidized Beds. Equation of Motion"* ,Indust. Engng. Chem.Fundam., Vol. 6, pp.527-539

Andrews IV, A.T., Loezos, P.N. and Sundaresan, S., 2005, *"Coarse-grid simulation of gas-particle flows in vertical risers"*, Ind. Eng. Chem. Res., Vol. 44, No. 16, pp. 6022-6037.

Bouillard, J.X., Lyczkowski, R.W. and Gidaspow, D., 1989, *"Porosity distributions in a fluidized bed with an immersed obstacle"*, AIChE J., Vol 35, No. 6, pp. 908-922

Campbell, C.S. and Wang, D.G., 1991, *"Particle pressure in gas-fluidized beds"*, J. Fluid Mech., Vol. 227, pp. 495-508.

Enwald, H., Peirano, E. and Almstedt, A.-E., 1996, *"Eulerian Two-Phase Flow Theory Applied to Fluidization"*, Int. J. of Multiphase Flow, Vol. 22, pp.21-66.

Garzó, V. and Dufty, J.W., 1999, *"Dense fluid transport for inelastic hard spheres"*, Phys. Rev. E, Vol. 59, pp. 5895–5911.

Gidaspow, D. and Ettehadieh, B., 1983, *"Fluidization in two-dimensional debs with a jet. Part II. Hydrodynamic modeling"*, Indust. Engng. Chem. Fundam., Vol. 22, pp. 193-201.

Gidaspow, D., 1994, *"Multiphase Flow and Fluidization"*, Academic Press, San Diego, CA, 407p.

Hrenya, C.M. and Sinclair, J.L., 1997, "Effects of particle-phase turbulence in gas-solid flows", AIChE Journal, Vol. 43, No. 4, pp. 853-869.

Igci, Y., Andrews IV, A.T., Sundaresan, S., Pannala, S. and O'Brien, T., 2008, *"Filtered two-fluid models for fluidized gas-particle suspensions"*, AIChE Journal, Vol. 54, No. 6, pp. 1431-1448.

Igci, Y. and Sundaresan, S., 2011a, *"Constitutive models for filtered two-fluid models of fluidized gas-particle flows"*, Ind. Eng. Chem. Res., Vol. 50, pp. 13190-13201.

Igci, Y. and Sundaresan, S., 2011b, *"Verification of filtered two-fluid models for gas-particle flows in risers"*, AIChE J., Vol. 57, pp. 2691-2707.

Jenkins, J.T. and Savage, S.B., 1983, *"A Theory for the Rapid Flow of Identical, Smooth, Nearly Elastic Spherical Particles"*, J. Fluid. Mech., Vol. 130, pp. 187-202.

Lun, C.K.K., Savage, S.B., Jeffrey, D.J. and Chepurniy, N., 1984, *"Kinetic Theories for Granular Flows: Inelastic Particles in Couette Flow and Singly Inelastic Particles in a General Flow Field"*, J. Fluid. Mech., Vol. 140, pp.223-256

Massoudi, M., Rajagopal, K.R., Ekmann, J.M. and Mathur, M.P., 1992, *"Remarks on the modeling of fluidized systems"*, AIChE J., Vol. 38, No. 3, pp. 471-472.

Mouallem, J., Chavez-Cussy N., Niaki R.A. , Milioli, C.C., Milioli, F.E., 2017 *"On the effects of the flow macro-scale over meso-scale filtered parameters in gas-solid riser flows"* submitted to AICHE Journal.

Milioli, C.C. and Milioli, F.E., 2011, *"On the sub-grid behavior of accelerated riser flows for a high Stokes number particulate"*, Industrial and Engineering Chemistry Research, Vol. 50, pp. 13538-13544.

Milioli, C.C., Milioli, F.E., Holloway, W., Agrawal, K. and Sundaresan, S., 2013, *"Filtered two-fluid models of fluidized gas-particle flows: New constitutive relations"*, AIChE J., Vol. 59, pp. 3265-3275.

Özel, A., Fede, P. and Simonin, O., 2013, *"Development of filtered Euler–Euler two-phase model for circulating fluidised bed: High resolution simulation, formulation and a priori analyses"*, Int. J. Multiphase Flow, Vol. 55 . pp. 43-63.

Parmentier, J-F, Simonin O. and Delsart O., 2012, *"A functional subgrid drift velocity model for filtered drag prediction in dense fluidized bed"*, AIChE J., Vol. 58, pp. 1084-1098.

Sarkar, A., Milioli, F.E., Ozarkar, S., Li, T., Sun, X. and Sundaresan, S., 2016, *"Filtered sub-grid constitutive models for fluidized gas-particle flows constructed from 3-D simulations"*, Chemical Engineering Science, Vol. 152, pp. 443-456.

Schneiderbauer, S. and Pirker, S., 2014, "Filtered and Heterogeneity-Based Subgrid Modifications for Gas–Solid Drag and Solid Stresses in Bubbling Fluidized Beds", AIChE J., Vol. 60, pp. 839-854.

Sinclair, J.L. and Jackson, R., 1989, *"Gas-particle flow in a vertical pipe with particle-particle interactions"*, AIChE Journal, Vol. 35, No. 9, pp. 1473-1486.

Sinclair, J.L., 1997, *"Hydrodinamic Modeling"* , In Circulating Fluidized Beds, ed. J.R. Grace et al., Chapman and Hall.

Cap. 5, p.149-180.

Syamlal, M., Rogers, W. and O'Brien, T. J., 1993, *"Theory guide"*, MFIX documentation, Vol. 1, DOE/METEC-94/1004 NTIS/DE9400087, National Technical Information Service, Springfield, VA.

Syamlal, M. 1998, *MFIX Documentation: Numerical Techniques*. DOE/MC-31346-5824. NTIS/DE98002029.

Tsuo, Y.P. and Gidaspow, D., 1990, *"Computation of flow patterns in circulating fluidized beds"*, AIChE J., Vol. 36, No. 6, pp. 885-896.

Wen, C.Y. and Yu, Y.U., 1966,*"Mechanics of fluidization"*, Chem. Engng. Prog. Symp. Series, Vol. 62, pp. 100-111.

7. RESPONSIBILITY NOTICE

The authors are the only responsible for the printed material included in this paper.